Final Report

Force Control of a Flexible Structure Mounted Manipulator

Theeraphong Wongratanaphisan
Department of Mechanical Engineering
Chiang Mai University

September 30th, 2007

Contract No. MRG4880198

Final Report

Force Control of a Flexible Structure Mounted Manipulator

Theeraphong Wongratanaphisan
Department of Mechanical Engineering
Chiang Mai University

Sponsered by
the Commission on Higher Education and the Thailand Research Fund

Acknowledgment

The author would like to express sincere appreciation toward the Thailand Research Fund and the Commission on Higher Education for financially supporting this research. The author wishes to thank the Department of Mechanical Engineering of Chiang Mai University for its full support in this project. Thank to Chansith Yodpruedtikarn who worked hard on getting the prototype robot and other hardware ready for experiment. Many thanks to Dr. Matthew O.T. Cole, the author's mentor, who has been giving valuable suggestions leading to the results of this research.

Abstract

This research investigates force control techniques for flexible structure mounted manipulators (FSMM) in contact tasks. The FSMM suffers from the dynamic complexity due to the flexibility of the structure that the manipulator is mounted to. These complications can get worse when the end-effector of the manipulator is in contact with environment because instability can occur. Here, two types of impedance control, force-based and position-based, for FSMM are investigated. The environment is assumed to be static. The analysis was carried out by deriving a one-dimensional contact model along the normal direction of the environment surface. Robust controllers were designed based on Nyquist stability criteria so that when in contact with static environment the system remains stable for all possible environment stiffnesses. In order to test the controllers, a 2-DOF lab-scale FSMM has been constructed. Experiments have been performed and the results show that the robust controllers can resolve the stability problems that occur under some conditions when non-robust controllers are used.

บทคัดย่อ

งานวิจัยนี้ศึกษาการควบคุมแรงของแขนกลยึดติดกับฐานที่เป็นโครงสร้างยืดหยุ่นในขณะมีการสัมผัสกับสิ่งแวดล้อม ระบบแขนกลนี้มีความยุ่งยากในการควบคุมเนื่องมาจากความยืดหยุ่นของฐาน และความยุ่งยากนี้อาจเพิ่มมากขึ้นอีกเมื่อปลายของแขนกลสัมผัสกับสิ่งแวดล้อมเนื่องจากระบบอาจสูญเสียเสถียรภาพ งานวิจัยนี้ได้ศึกษาการควบคุมแบบอิมพีแดนซ์ (impedance control) 2 ชนิดคือ ชนิดที่อ้างอิงกับแรง (force-based) และ ชนิดที่อ้างอิงกับตำแหน่ง (position-based) โดยสิ่งแวดล้อมที่มีการสัมผัสกับแขนกลถูกสมมุติให้ไม่มีการเคลื่อนไหว (static) พื้นฐานของการวิเคราะห์มาจากการสร้างแบบจำลองทางคณิตศาสตร์ของการสัมผัสแบบ 1 มิติตามแนวตั้งฉากพื้นผิวสัมผัส จากนั้นตัวควบคุมแบบ robust ถูกแบบโดยอ้างอิงกับเกณฑ์เสถียรภาพแบบ Nyquist ซึ่งตัวควบคุมนี้สามารถรักษาเสถียรภาพของระบบได้ตลอดทุกค่าความยืดหยุ่นของสิ่งแวดล้อม เพื่อทดสอบการทำงานของตัวควบคุมที่ได้ออกแบบ แขนกลจำลองขนาดเล็กแบบ 2 องศาอิสระได้ถูกสร้างขึ้น และจากการทดสอบ ผลการทดลองบ่งชี้ให้เห็นถึงความสามารถในการรักษาเสถียรภาพของระบบเมื่อควบคุมด้วยตัวควบคุมแบบ robust

Executive Summary

Flexible structure mounted manipulator (FSMM) is a class of robot manipulator system that consists of a rigid manipulator mounted on the structure that is normally large and not rigid. The FSMM finds applications in the nuclear waste remediation and has potentials for use in large structure inspection tasks such as buildings, highways and bridges. In the course of manipulator motion, reactive forces are transferred through the structure and vibrations occur. These vibrations can cause further complication when the manipulator is in contact with environment. This research studies force control for this type of manipulator when in contact with static environment. The focus of the control methods is on the impedance control where the relationship between the external force and the end-effector displacement is defined and the robot is controlled accordingly. The goal is for the system to perform according to the desired impedance while remain stable when in contact with static environment such as wall. The study involves modeling of the system in contact tasks as one dimension problem and based on the one-dimensional model robust controllers are designed based on Nyquist criteria. Two robust controllers have been derived: 1) position-based impedance control and 2) force-based impedance control. In order to verify the control schemes, a 2-DOF lab-scale FSMM has been constructed. Tests have been performed and the results show that the robust controllers can resolve the stability problems that occur under some conditions when non-robust controllers are used. This research can be studied further in a number of topics such as robust performance during contact, joint flexibility, dynamic environment and friction.

Chapter 1

Introduction

1.1 Statement of the Problem

Flexible structure mounted manipulator (FSMM) is a class of robot manipulator system that consists of a rigid manipulator mounted on the structure that is not rigid as shown in fig. 1.1. This system also includes a micro-macro manipulator (MMM) system in which a smaller (micro) manipulator, considered rigid, is mounted on the tip of a bigger (macro) manipulator, considered flexible. The MMM is capable of operating in tasks that cover large working area. Here, the macro manipulator has long arm and hence provides large working space. However, due to structural flexibility its end-point can not be positioned accurately. During operation, the macro manipulator is employed for coarse positioning of the micro manipulator which then operates in a narrower region with more accuracy. In each coarse positioning, the macro manipulator holds its posture until the micro manipulator finishes its tasks. Then the macro manipulator changes it posture to relocate the micro manipulator, and the operation continues.

There has been much research work on various aspects of typical robot manipulators that are mounted on a rigid base. However, FSMM only attracts few researchers. Much of the research in FSMM is carried out if not on an existing systems then for the sake of individual interest. This is due to the particularity of the system. Nevertheless, studying the behaviors of the FSMM can be beneficial for understanding the effects of vibration exists in a robot system. So far the

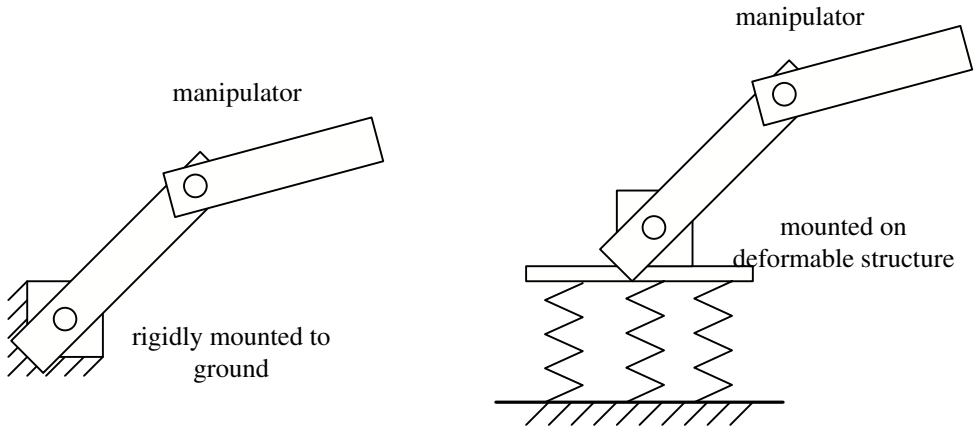

a) typical robot manipulator b) FSMM

Figure 1.1: a) typical robot manipulator b) flexible structure mounted manipulator

FSMM finds applications in space robotics and nuclear waste remediation areas. It also has potential for use in large structure inspection tasks such as buildings, highways and bridges.

There are two aspects in terms of controlling a robot system, : 1) position control and 2) forces control. Position control basically deals with the accuracy of the end-effector while force control deals with controlling the forces exerted on the end-effector and stability of the system. When the robot is in contact with the environment its dynamics changes and with closed loop control, the system can become unstable. Therefore in the tasks that require the robot to touch the environment, the controllers must be designed such that stability is preserved. This research aims to study force control of FSMM when it is in contact with static environment.

1.2 Reviews on Control of FSMM

There are basically two approaches for dealing with vibration in the FSMM: 1) vibration avoidance and 2) vibration damping. In the first approach, the manipulator is controlled such that little or no vibration occurs. Two main techniques are within this category: path planning and input shaping. In path planning, the goal is to plan the path for the manipulator to move so that the reaction force

transferred to the base is minimal. Sagli and Egeland [6] proposed the conservation of coupling momentum that eliminates the dynamic coupling between the end-effector and the structure in a redundant manipulator system. Nenchev and Yoshida [5]proposed a similar scheme called the conservation of coupling momentum. Torrest and Dubowsky [9] proposed a technique that controls strain energy in the flexible structure which is presented in the form of manipulator motion by contour mapping.

In input shaping, the idea is to filter the reference command so that the frequency contents that match the natural frequencies of the system are eliminated. Magee and Book [4] have used this technique to reduce vibration in FSMM. Kwon et al. [1] studied several filters in input shaping techniques for large-scale manipulator used in nuclear waste management. In vibration damping approach, the goal is to damp out vibrations that occur in the system quickly. Yoshida et al. [11] proposed an inertial damping technique with is a vibration damping approach for FSMM. Scott and Gilbert [7] used this technique for vibration control in space manipulator.

As oppose to position control, the force control problem has not been widely studied and so there are many topics to be explored. This study investigates control schemes for FSMMs which performs tasks that require the end-effector to be in contact with static environment.

1.3 Objectives of study

This research aims to study force control of the FSMM when performs tasks that require contact with static environment. The goal is to design controllers such that the system remains stable for a wide range of stiffness of the static environment.

Chapter 2

Dynamics of a Flexible Structure Mounted Manipulator in Contact Tasks

2.1 Equations of Motion of Robot Manipulator

Let $\theta \in \Re^{n\times 1}$ denote the vector of containing the joint angles of the rigid manipulator and $X \in \Re^{m\times 1}$ denote the $m\,(\leq 6)$-dimensional task space vector of the end-effector of the manipulator. $\Re^{n\times 1}$ represents n-dimensional Euclidean space. X is called the "**manipulation vector**".

The manipulation vector is related to the joint angles by

$$X = f(\theta) \tag{2.1}$$

The first and second derivatives of X are

$$\dot{X} = J(\theta)\dot{\theta} \tag{2.2}$$

and

$$\ddot{X} = J\ddot{\theta} + \dot{J}\dot{\theta} \tag{2.3}$$

where J is the Jacobian matrix. The equation of motion of a robot manipulator

is given by

$$M(\theta)\ddot{\theta} + N(\theta, \dot{\theta}) + G(\theta) = \tau + \tau_e \tag{2.4}$$

where θ is the joint angles vector

$M(\theta)$ is the mass matrix

$N(\theta, \dot{\theta})$ is the Colioris and centrifugal forces vector

$G(\theta)$ is the gravirational forces vector

τ is the actuator torque vector

τ_e is a vector containing the external forces

2.2 Equations of Motion of FSMM

Let $q \in \Re^{(n+p)\times 1}$ denote the vector of containing the joint angles of the rigid manipulator, $\theta \in \Re^{r\times 1}$, and the states of the flexible structure ζ. The states of the flexible structure, ζ, can be obtained from a finite dimension approximation of the flexible modes of the structure.

The manipulation vector is related to the joint angles and the flexible structure states by

$$X = f(q) = f(\theta, \zeta) \tag{2.5}$$

The first and second derivatives of X are

$$\begin{aligned} \dot{X} &= J(q)\dot{q} \\ &= J_\theta(\theta, \zeta)\dot{\theta} + J_\zeta(\theta, \zeta)\dot{\zeta} \end{aligned} \tag{2.6}$$

and

$$\begin{aligned} \ddot{X} &= J\ddot{q} + \dot{J}\dot{q} \\ &= J_\theta\ddot{\theta} + J_\zeta\ddot{\zeta} + \dot{J}_\theta\dot{\theta} + \dot{J}_\zeta\dot{\zeta} \end{aligned} \tag{2.7}$$

where J_θ and J_ζ are Jacobian matrices of appropriate dimension. Note that $J(q) = [J_\theta \;\; J_\zeta]$.

The equation of motion of a FSMM is given by

$$M(q)\ddot{q} + N(q,\dot{q}) + G(q) = \tau + \tau_e \tag{2.8}$$

where q is a vector containing the states of the base vibration, ζ, and the manipulator joint angles, θ

$M(q)$ is the mass matrix

$N(q,\dot{q})$ is a vector containing the Colioris forces

$G(q)$ is the gravirational forces vector

τ is the actuator forces vector

τ_e is the external forces vector

When the end-effector contacts the environment, the contact forces, f_e, are related to the effective torque by

$$\tau_e = J^T f_e \tag{2.9}$$

During contact, the behaviors of the FSMM can change reasonably due to the changes in boundary condition of the system. In general, the contact force is a function of the joint angles, flexible structure states and the parameters of the environment such as stiffness and damping. In a more complicated system, the environment can itself be a dynamics system but this case is out of the scope of this study.

Chapter 3

Impedance Control for Flexible Structure Mounted Manipulators in Contact Tasks

Impedance control is a unified position-force control approach that suits manipulator performing contact tasks. In this control scheme, rather than regulating the end-effector positions and/or forces, the impedance between the end-effector displacement, δx_e, and acting forces, f_e, is defined. The manipulator is so controlled such that the desired impedance is achieved. Normally, the desired impedance is in the form of a spring-mass-damper system, i.e.,

$$f_e = M_d \ddot{x}_e + B_d \delta \dot{x}_e + K_d \delta x_e \tag{3.1}$$

where M_d, B_d and K_d are the desired mass, damping coefficient and K_d stiffness matrices, respectively. The manipulator dynamic is represented by

$$M(\theta)\ddot{\theta} + N(\theta, \dot{\theta}) + G(q) = \tau + J^T(\theta) f_e \tag{3.2}$$

and the end-effector velocities are related to the manipulator joint velocities by

$$\dot{x}_e = J(\theta)\dot{\theta} \tag{3.3}$$

and

$$\ddot{x}_e = J(\theta)\ddot{\theta} + \dot{J}(\theta)\dot{\theta} \tag{3.4}$$

There are two types of impedance controls: 1) force-based impedance control and 2) position-based impedance control. In the force-based scheme, the control force is calculated directly from the dynamic of the manipulator and the desired impedance. In the position-based scheme, the main control is based on position servo control. The desired impedance is achieved through adjustment of the position reference.

3.1 Force-Based Impedance Control for Robot Manipulators

For brevity, a function $y(\theta)$ or $y(\theta, \dot{\theta})$ will be written as y. Substituting eqs. 3.1 and 3.2 into eq. 3.4 yields,

$$M_d^{-1}\left(f_e - B_d\delta\dot{x}_e - K_d\delta x_e\right) = JM^{-1}\left(\tau + J^T f_e - N - G\right) + \dot{J}\dot{\theta}$$

or

$$JM^{-1}\tau = \left(M_d^{-1} - JM^{-1}J^T\right) f_e - M_d^{-1}\left(B_d\delta\dot{x}_e + K_d\delta x_e\right) + JM^{-1}\left(N + G\right) - \dot{J}\dot{\theta}$$

In terms of the effective forces from actuators seen at the end-effector, f_a

$$\begin{aligned} JM^{-1}J^T f_a &= \left(M_d^{-1} - JM^{-1}J^T\right) f_e - M_d^{-1}\left(B_d\delta\dot{x}_e + K_d\delta x_e\right) \\ &\quad + JM^{-1}\left(N + G\right) - \dot{J}\dot{\theta} \end{aligned}$$

or

$$\begin{aligned} f_a &= \left(\tilde{M}M_d^{-1} - I\right) f_e - \tilde{M}M_d^{-1}\left(B_d\delta\dot{x}_e + K_d\delta x_e\right) \\ &\quad + \tilde{M}JM^{-1}\left(N + G\right) - \tilde{M}\dot{J}\dot{\theta} \end{aligned}$$

where $\tilde{M} = \left(JM^{-1}J^T\right)^{-1}$ is the matrix called the "**mobility tensor**". In turn, the actuator torques are obtained from

$$\begin{aligned} \tau &= J^T\left(\tilde{M}M_d^{-1} - I\right) f_e - J^T\tilde{M}M_d^{-1}\left(B_d\delta\dot{x}_e + K_d\delta x_e\right) \\ &\quad + J^T\tilde{M}JM^{-1}\left(N + G\right) - J^T\tilde{M}\dot{J}\dot{\theta} \end{aligned} \tag{3.5}$$

With the control law in eq. 3.5, the manipulator considered at the end-effector will behave exactly according to the desired impedance described in eq. 3.1.

Impedance Control for Manipulators in contact Tasks

In contact tasks, the manipulator is normally operating at slow speed. Then the equations of motion can be represented in a much simple form by neglecting some higher order terms such as the Coriolis and centrifugal forces. In this case, the control law in eq. 3.5 may be approximated by

$$\tau = J^T \left(\tilde{M} M_d^{-1} - I \right) f_e - J^T \tilde{M} M_d^{-1} \left(B_d \delta \dot{x}_e + K_d \delta x_e \right) + J^T \tilde{M} J M^{-1} G \qquad (3.6)$$

3.2 Position-Based Impedance Control for Robot Manipulators

From the equation of motion,

$$M(q)\ddot{\theta} + N(\theta, \dot{\theta}) + G(q) = \tau + J^T(\theta) f_e$$

We may write the control torque $\tau = J^T f_a$ where f_a is the control forces seen at the end-effector. In this scheme, f_a is given in the servo control form:

$$f_a = G_s(X_r - X_e) + \tilde{M} J M^{-1}(N + G) - \tilde{M} \dot{J} \dot{\theta} \qquad (3.7)$$

where X_r is the adjusted position reference command and G_s is the servo controller. With this control forces, the equations of motion becomes

$$\tilde{M} \ddot{X}_e = G_s(X_r - X_e) + f_e$$

or

$$X_r = G_s^{-1} \tilde{M} \ddot{X}_e + X_e - G_s^{-1} f_e$$

Let X_0 be the position reference command. Then the position reference adjustment is given by

$$\begin{aligned} \Delta X &= X_r - X_0 \\ &= G_s^{-1} \tilde{M} \ddot{X}_e + X_e - G_s^{-1} f_e - X_0 \end{aligned}$$

or in Laplace domain

$$\Delta X = \left(G_s^{-1} \tilde{M} s^2 + I \right) X_e - G_s^{-1} f_e - X_0 \qquad (3.8)$$

But from the desired impedance,

$$M_d s^2 X_e + (B_d s + K_d)(X_e - X_0) \;=\; F_e$$

Then

$$X_e = \left(M_d s^2 + B_d s + K_d\right)^{-1} \left(F_e - (B_d s + K_d) X_0\right) \tag{3.9}$$

Substituting eq. 3.9 into eq. 3.8 yields

$$\begin{aligned} \Delta X \;=\; & \left[\left(G_s^{-1}\tilde{M}s^2 + I\right)\left(M_d s^2 + B_d s + K_d\right)^{-1} - G_s^{-1}\right] F_e \\ & - \left[\left(G_s^{-1}\tilde{M}s^2 + I\right)\left(M_d s^2 + B_d s + K_d\right)^{-1}(B_d s + K_d) + I\right] X_0 \end{aligned}$$

Therefore, the force filter should take the form

$$\Delta X = G_f F_e$$

where

$$G_f = \left(G_s^{-1}\tilde{M}s^2 + I\right)\left(M_d s^2 + B_d s + K_d\right)^{-1} - G_s^{-1} \tag{3.10}$$

In eq. 3.7, X_r can be written as

$$X_r = X_0 + \Delta X = X_0 + G_f F_e$$

By substituting eq. 3.10 into eq. 3.7 we obtain the force control law as seen at the end-effector

$$\begin{aligned} F_a \;=\; & \left(\left(\tilde{M}s^2 + G_s\right)\left(M_d s^2 + B_d s + K_d\right)^{-1} - I\right) F_e - G_s(X_e - X_0) \\ & + \tilde{M} J M^{-1}(N + G) - \tilde{M}\dot{J}\dot{\theta} \end{aligned}$$

or in term of control torque

$$\begin{aligned} \tau \;=\; & J^T\left(\left(\tilde{M}s^2 + G_s\right)\left(M_d s^2 + B_d s + K_d\right)^{-1} - I\right) F_e - J^T G_s(X_e - X_0) \\ & + J^T \tilde{M} J M^{-1}(N + G) - J^T \tilde{M}\dot{J}\dot{\theta} \end{aligned}$$

Similarly, for contact problem the Colioris and centrifugal force terms may be dropped, i.e.,

$$\tau = J^T\left(\left(\tilde{M}s^2 + G_s\right)\left(M_d s^2 + B_d s + K_d\right)^{-1} - I\right) F_e - J^T G_s(X_e - X_0)$$

When the manipulator is in contact with the environment, in respect to contact forces the problem can be reduced to one dimension, namely, the surface normal direction. In the following sections, the analysis will focus on developing one dimensional contact model applicable to impedance control of the FSMM. In the analysis, the model will not include the gravity terms as they do not have influences on the dynamics of the system. For completeness, the gravity can be easily included by following similar analysis presented below.

3.3 Impedance Control and One-Dimensional Contact Model for a FSMM

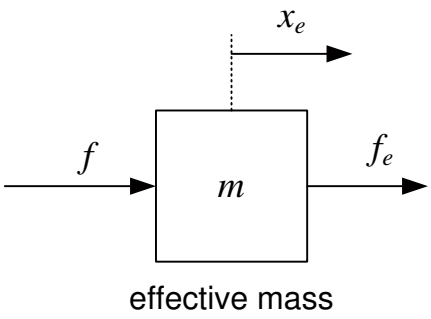

Figure 3.1: A simple mass model

Consider the end-effector dynamics represented by a simple mass m, actuated by an actuator with effective force f and interacts with the environment with external force f_e as shown in fig. 3.1. x_e is the displacement of the mass. The equation of motion of the mass is given by

$$m\ddot{x_e} = f + f_e \tag{3.11}$$

Suppose that we would like the system to behave according the desired impedance described by

$$f_e = m_d\ddot{x_e} + b_d\delta\dot{x_e} + k_d\delta x_e \tag{3.12}$$

or

$$\ddot{x_e} = \frac{1}{m_d}\left(f_e - b_d\delta\dot{x_e} - k_d\delta x_e\right) \tag{3.13}$$

Substituting eq. 3.13 into eq. 3.11 yields

$$\begin{aligned} \frac{m}{m_d}\left(f_e - b_d\delta\dot{x_e} - k_d\delta x_e\right) &= f + f_e \\ f &= -\frac{m}{m_d}\left(b_d\delta\dot{x_e} + k_d\delta x_e\right) + \left(\frac{m}{m_d} - 1\right) f_e \end{aligned} \quad (3.14)$$

or in Laplace domain;

$$F(s) = -\frac{m}{m_d}\left(b_d s + k_d\right)\delta X_e(s) + \left(\frac{m}{m_d} - 1\right) F_e(s) \quad (3.15)$$

By substituting the force according to the control law in eq. 3.14, the mass will behave according to the desired impedance in eq. 3.12.

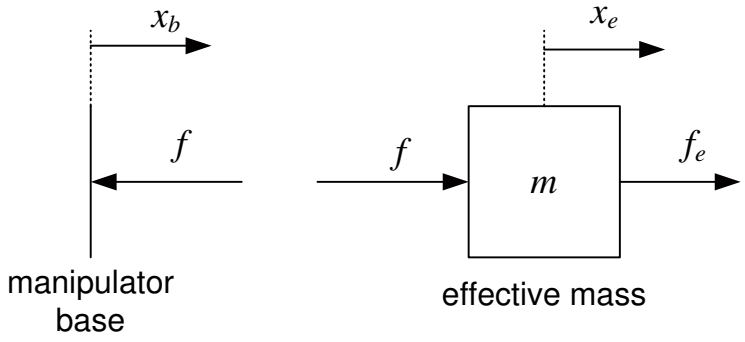

Figure 3.2: One-DOF model of FSMM

Effect of Base Motion

For the FSMM consider the 1-DOF model shown in fig. 3.2. The manipulator base motion is described by $x_b(t)$. Here, the reactive force due to the actuator force applied to the effective mass acting on the flexible base in the opposite direction. This reactive force can cause vibration in the system. Let the relation between the reactive force and the manipulator base be described by

$$X_b(s) = -G_b(s)F(s) \quad (3.16)$$

To employ the impedance controller to the FSMM, consider the form of control law similar to eq. 3.14:

$$F(s) = -\frac{m}{m_d}\left(b_d s + k_d\right)\delta X_m(s) + \left(\frac{m}{m_d} - 1\right) F_e(s) \quad (3.17)$$

Here the total displacement $\delta X_e(s)$ is replaced by the measured displacement $\delta X_m(s)$. Typically, the position of the robot's end-effector is calculated from the joint sensor data with respect to the base. Therefore, when $X_b \neq 0$ the measured displacement is not the total displacement but instead a relative displacement: $\delta X_m(s) = \delta X_e(s) - X_b(s)$. Thus,

$$F(s) = -\frac{m}{m_d}\left(b_d s + k_d\right)\left(\delta X_e(s) - X_b(s)\right) + \left(\frac{m}{m_d} - 1\right) F_e(s) \tag{3.18}$$

Let $K(s) = b_d s + k_d$. With the base motion described in eq. 3.16

$$\begin{aligned} F(s) &= -\frac{m}{m_d} K(s)\left(\delta X_e(s) + G_b(s)F(s)\right) + \left(\frac{m}{m_d} - 1\right) F_e(s) \\ \left(1 + \frac{m}{m_d} K(s) G_b(s)\right) F(s) &= -\frac{m}{m_d} K(s)\delta X_e(s) + \left(\frac{m}{m_d} - 1\right) F_e(s) \end{aligned}$$

or

$$F(s) = \left(1 + \frac{m}{m_d} K(s) G_b(s)\right)^{-1} \left[-\frac{m}{m_d} K(s)\delta X_e(s) + \left(\frac{m}{m_d} - 1\right) F_e(s)\right] \tag{3.19}$$

or

$$F(s) = G_x(s)\delta X_e(s) + G_f(s) F_e(s) \tag{3.20}$$

where

$$G_x(s) = -\left(1 + \frac{m}{m_d} K(s) G_b(s)\right)^{-1} \frac{m}{m_d} K(s) \tag{3.21}$$

$$\text{and} \quad G_f(s) = \left(1 + \frac{m}{m_d} K(s) G_b(s)\right)^{-1} \left(\frac{m}{m_d} - 1\right) \tag{3.22}$$

With this control law, the equation of motion becomes

$$\begin{aligned} m s^2 X_e(s) &= G_x(s)\delta X_e(s) + G_f(s) F_e(s) + F_e(s) \\ \left(m s^2 - G_x(s)\right)\delta X_e(s) &= \left(1 + G_f(s)\right) F_e(s) \\ \frac{\delta X_e(s)}{F_e(s)} &= \frac{1 + G_f(s)}{m s^2 - G_x(s)} \\ &= \frac{\frac{m}{m_d} K(s) G_b(s) + \frac{m}{m_d}}{m s^2 \left(1 + \frac{m}{m_d} K(s) G_b(s)\right) + \frac{m}{m_d} K(s)} \\ \frac{\delta X_e(s)}{F_e(s)} &= \frac{1}{m s^2} \frac{1 + K(s) G_b(s)}{\frac{m_d}{m} + \frac{K(s)}{m s^2} + K(s) G_b(s)} \end{aligned} \tag{3.23}$$

Here, transfer function $\delta X_e(s)/F_e(s)$, the admittance of the system, contains function $G_b(s)$. When $G_b(s) = 0$ the impedance of the system is exactly the desired impedance.

3.4 Impedance Control with Base Acceleration Measurement

Consider the control low:

$$F(s) = -\frac{m}{m_d}K(s)\delta X_m(s) + \left(\frac{m}{m_d} - 1\right)F_e(s) + D(s)s^2X_b(s) \tag{3.24}$$

This control is similar to the previous control law except the addition of the term $D(s)s^2X_b(s)$. $s^2X_b(s)$ is the acceleration of the base and $D(s)$ is the acceleration filter to be designed. For $X_b(s) = -G_b(s)F(s)$,

$$\begin{aligned}
F(s) &= -\frac{m}{m_d}K(s)\left(\delta X_e(s) - X_b(s)\right) + \left(\frac{m}{m_d} - 1\right)F_e(s) + D(s)s^2X_b(s) \\
&= -\frac{m}{m_d}K(s)\left(\delta X_e(s) + G_b(s)F(s)\right) + \left(\frac{m}{m_d} - 1\right)F_e(s) - D(s)s^2G_b(s)F(s) \\
F(s) &= -\left(1 + \frac{m}{m_d}K(s)G_b(s) + D(s)s^2G_b(s)\right)^{-1}\frac{m}{m_d}K(s)\delta X_e(s) \\
&\quad + \left(1 + \frac{m}{m_d}K(s)G_b(s) + D(s)s^2G_b(s)\right)^{-1}\left(\frac{m}{m_d} - 1\right)F_e(s)
\end{aligned}$$

Substituting into eq. 3.11 and rearranging yields

$$\frac{\delta X_e(s)}{F_e(s)} = \frac{1}{ms^2}\frac{1 + \left(K(s) + \frac{m_d}{m}D(s)s^2\right)G_b(s)}{\frac{m_d}{m} + \frac{K(s)}{ms^2} + \left(K(s) + \frac{m_d}{m}D(s)s^2\right)G_b(s)}$$

Ideally, if the acceleration filter is designed such that

$$D(s) = -\frac{m}{m_d}\frac{K(s)}{s^2} \tag{3.25}$$

the resulting transfer function would be the ideal one, i.e.,

$$\frac{\delta X_e(s)}{F_e(s)} = \frac{1}{\frac{m_d}{m} + \frac{K(s)}{ms^2}}$$

The filter $D(s)$ in eq. 3.25 actually compensates for the base motion by double integrating the acceleration signal to obtain the base motion. However, in practice such filter will have drift problem. To cope with the drift problem, the filter can be modified to

$$D(s) = -\frac{m}{m_d}\frac{K(s)}{(s+a)^2} \tag{3.26}$$

where a is a small positive real value.

3.5 Robust Force-Based Impedance Control for FSMM in Contact Tasks

In this section we derive the robust solution in case that $G_b(s)$ is not known. The goal is to arrive at the controller that is robust against the base vibration with certain bound on $G_b(j\omega)$. From eq. 3.23:

$$\begin{aligned} T_{fb}(s) = \frac{\delta X_e(s)}{F_e(s)} &= \frac{1}{ms^2}\frac{1+K(s)G_b(s)}{\frac{m_d}{m}+\frac{K(s)}{ms^2}+K(s)G_b(s)} \\ &= \frac{1}{ms^2}\frac{1+K(s)G_b(s)}{A(s)+K(s)G_b(s)} \end{aligned} \tag{3.27}$$

where

$$A(s) = \frac{m_d}{m} + \frac{K(s)}{ms^2} \tag{3.28}$$

Assume that the system is stable in non-contact operation. When the end-effector is in contact with wall (stiffness k_w), the condition for global stability during contact is that $T(j\omega)$ must not cross the negative real axis for all ω. This will happen when

$$T(j\omega) = -\frac{1}{m\omega^2}\frac{1+K(j\omega)G_b(j\omega)}{A(j\omega)+K(j\omega)G_b(j\omega)} = -\alpha$$

where α is a positive scalar. Equivalently, if there exists some $\omega > 0$ such that

$$\angle\left(A(j\omega)+K(j\omega)G_b(j\omega)\right) = \angle\left(1+K(j\omega)G_b(j\omega)\right)$$

Thus, contact stability requires that

$$\angle\left(A(j\omega)+K(j\omega)G_b(j\omega)\right) \neq \angle\left(1+K(j\omega)G_b(j\omega)\right), \quad \forall\omega > 0 \tag{3.29}$$

Now let us suppose that $K(j\omega)G_b(j\omega)$ is bounded by a frequency dependent scalar $g(\omega)$ according to:

$$|K(j\omega)G_b(j\omega)| < g(\omega) \tag{3.30}$$

Then stability requires that

$$\angle\left(A(j\omega)+e^{j\phi}g(\omega)\right) \neq \left(1+e^{j\phi}g(\omega)\right), \quad \forall\omega > 0, \phi \tag{3.31}$$

For positive (dissipative) transfer function $K(s)$ as $\omega \to \infty$

$$\frac{K(j\omega)}{m\omega^2} \to 0 \quad \text{and then} \quad A(j\omega) = -\frac{K(j\omega)}{m\omega^2} + \frac{m_d}{m} \to \frac{m_d}{m}$$

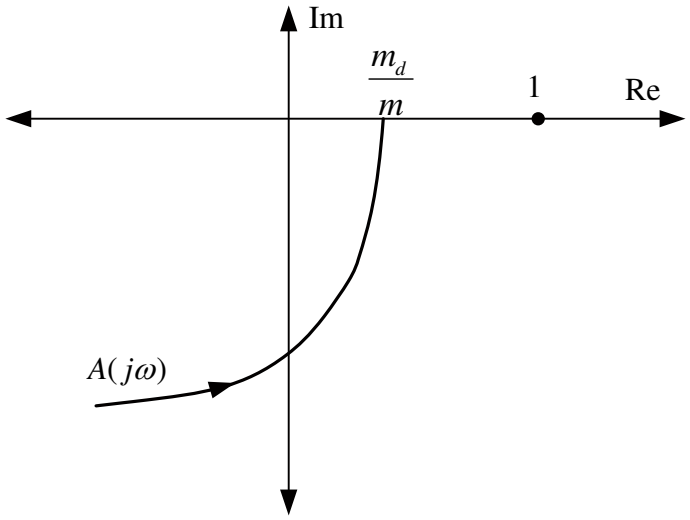

Figure 3.3: Typical plot of $A(j\omega)$

An example plot of $A(j\omega)$ over the range of ω for typical $K(s)$ is shown in fig. 3.3. At $\omega = \omega_0$, consider circle with radius $g(\omega)$ which represents the bound of the magnitude of $K(j\omega)G_b(j\omega)$. From eq. 3.31, the stability condition can be observed for 3 cases as shown in fig. 3.4 to fig 3.6. For $\theta = -\angle A(j\omega_0) - \angle(1 - A(j\omega_0))$

Case 1 Re$(A(j\omega)) < 1$ **and** $\theta < 90^\circ$

According to eq. 3.31, for $\mathrm{Re}(A(j\omega)) < 1$ and $\theta < 90^\circ$ the bound of uncertainty in eq. 3.30 is given by

$$|K(j\omega)G_b(j\omega)| < g(\omega) = \min\left(|A(j\omega)|, 1\right) \tag{3.32}$$

Case 2 Re$(A(j\omega)) < 1$ **and** $\theta > 90^\circ$

In this case, the bound of uncertainty in eq. 3.30 is given by

$$|K(j\omega)G_b(j\omega)| < g(\omega) = |A(j\omega)| \sin\theta \tag{3.33}$$

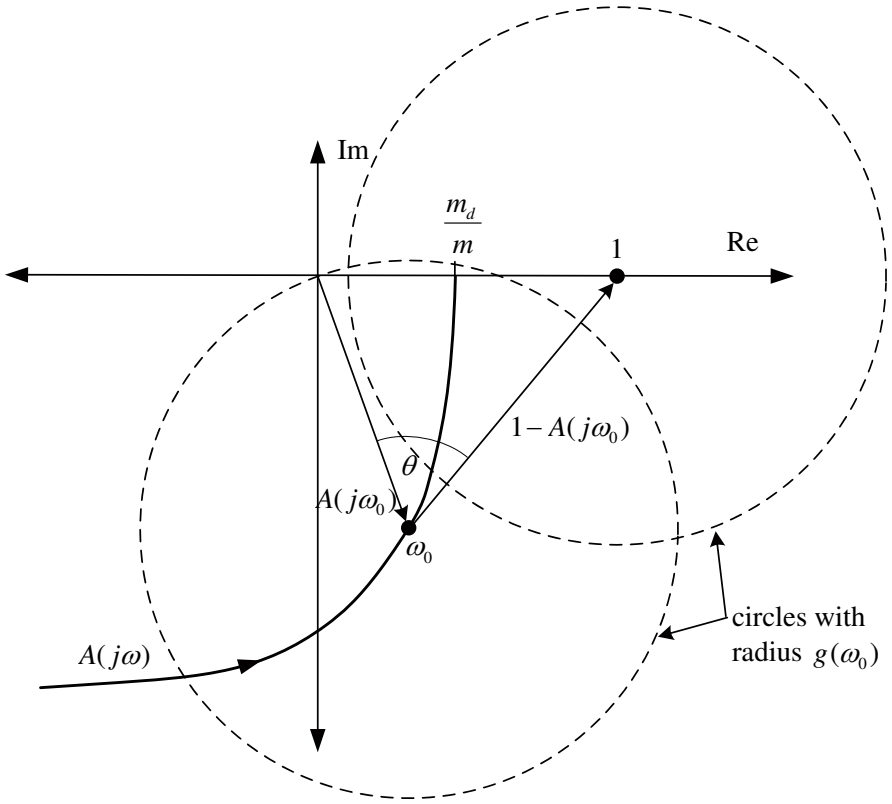

Figure 3.4: Bound on $G_b(j\omega)$: Re$(A(j\omega))$<1 and $\theta < 90°$ (case 1)

Case 3 Re$(A(j\omega)) > 1$

Similar to case 2, the bound of uncertainty in this case is given by

$$|K(j\omega)G_b(j\omega)| < g(\omega) = |A(j\omega)| \sin\theta \tag{3.34}$$

We are interested in the behavior of this bound at frequencies where we would expect $|K(j\omega)G_b(j\omega)|$ to be large due to natural modes of vibration of the system base. If ω_{nd} is the natural frequency/bandwidth of the impedance control law,

Then for $\omega \gg \omega_{nd}$,

$$A(j\omega) = -\frac{K(j\omega)}{m\omega^2} + \frac{m_d}{m} \approx \frac{m_d}{m}$$

So, in the frequency range $\omega \gg \omega_{nd}$, the robust stability condition is

$$|K(j\omega)G_b(j\omega)| < \left|\frac{m_d}{m}\right| \sin\theta$$

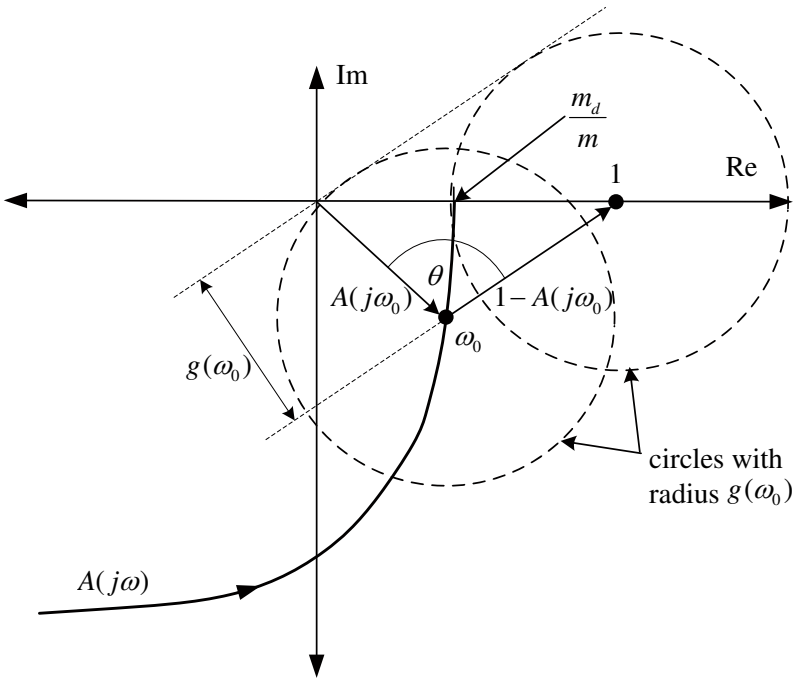

Figure 3.5: Bound on $G_b(j\omega)$: Re$(A(j\omega))$<1 and $\theta > 90°$ (case 2)

Robust controller design

Consider the control law:

$$F(s) = -\frac{m}{m_d}Q(s)^{-1}K(s)\left(\delta X_e(s) - X_b(s)\right) + \left(\frac{m}{m_d}Q^{-1}(s) - 1\right)F_e(s) \qquad (3.35)$$

This control law is similar to the one expressed in eq. 3.18 except an extra term $Q^{-1}(s)$ which multiplies $\frac{m}{m_d}$. With this control law, one can obtain the same form transfer function in eq. 3.27:

$$T_{fb}(s) = \frac{\delta X_e(s)}{F_e(s)} = \frac{1}{ms^2}\frac{1 + K(s)G_b(s)}{A(s) + K(s)G_b(s)}$$

except now

$$A(s) = \frac{K(s)}{ms^2} + \frac{m_d}{m}Q(s) \qquad (3.36)$$

The filter $Q(s)$ can be used to increase robustness of the system. It can be designed such that the magnitude of its frequency response function is small in the range where G_b is expected to be large, i.e. at the natural frequencies of G_b and also to keep the angle $\theta = \angle(1 - A(j\omega)Q(j\omega))$ as close to 90° as possible of for wide range of ω. Consider Q in the form of a lag-compensator

$$Q(s) = \frac{\tau_1 s + 1}{\tau_2 s + 1}$$

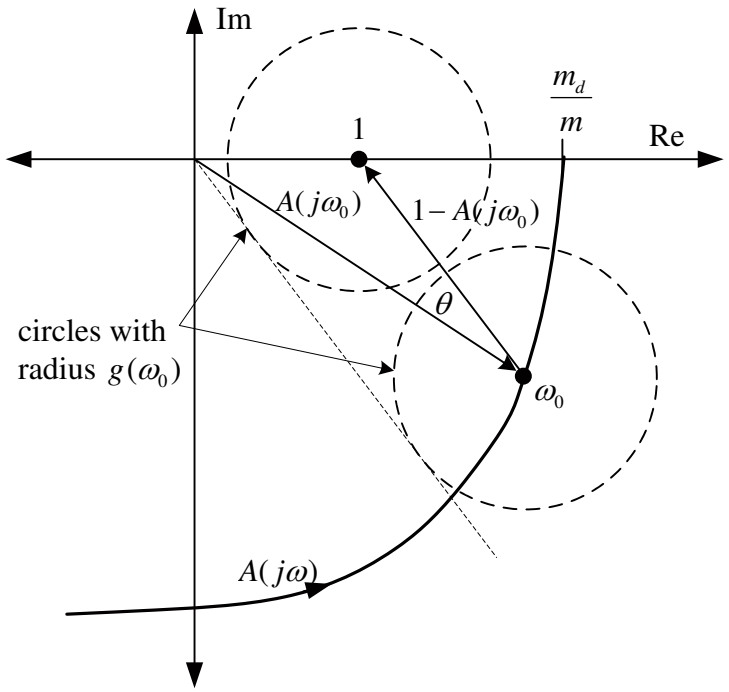

Figure 3.6: Bound on $G_b(j\omega)$: Re$(A(j\omega))>1$ (case 3)

with $\tau_1 < \tau_2$. Here, $|Q(j\omega)|$ will drops below 1 after the corner frequency $\omega_a = 1/\tau_2$ with the rate of -20 dB/decade and will remain constant after $\omega_b = 1/\tau_1$. We can select τ_2 such that ω_a is less than the first natural frequency of the base. The lag compensator Q will also help to keep the angle θ larger when ω increases, thus providing robustness.

As an example, consider the system with $m = 10, m_d = 1, b_d = 1.4, k_d = 1$. Figure 3.7 shows plots of $A(j\omega)$ with and without filter $Q = \frac{0.01s+1}{0.1s+1}$ over the frequency range $\omega = [1, \infty]$. With the filter $Q(s)$, $A(j\omega)$ approaches the real axis more slowly which will keep θ in ineq. 3.33 going to 180° more slowly. Figure 3.8 shows plot of $T_{fb}(j\omega)$ for impedance control with and without $Q(s)$ for $G_b = \frac{1}{15s^2+150s+37500}$. Here without $Q(s)$ the Nyquist plot of $T_{fb}(s)$ crosses the negative real axis. Therefore, the system can be unstable for some values of wall stiffness. On the other hand, with $Q(s)$ the Nyquist plot of $T_{fb}(s)$ does not the negative real axis and therefore the system will be stable throughout the range of wall stiffness.

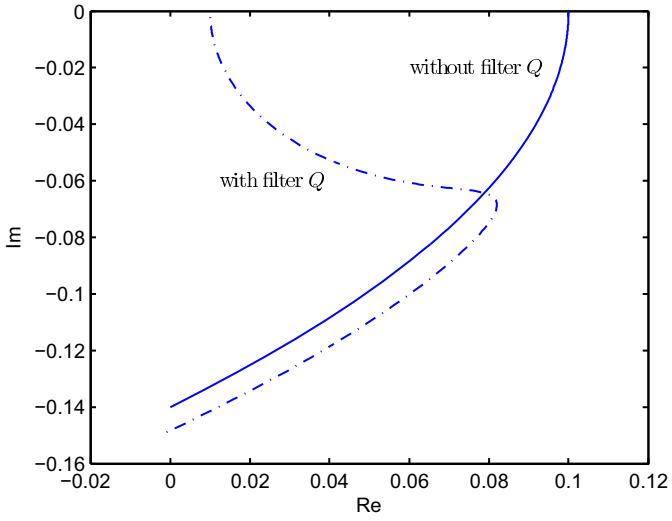

Figure 3.7: Plot of $A(j\omega)$ (for $m = 10, m_d = 1, b_d = 1.4, k_d = 1, Q = (0.01s + 1)/(0.1s + 1)$)

3.6 Robust Position-Based Impedance Control for FSMM

Figure 3.9 shows the diagram of a position-based impedance control scheme for a typical robot manipulator. G_m is the transfer function between the robot end-effector position and the actuator force. G_e is transfer function representing the dynamic of the environment. G_f is the force filter and G_s is the transfer function of the servo controller.

From the block diagram

$$\begin{aligned} F &= G_s(X_r - X_e) \\ &= G_s(X_0 + \Delta X_0 - X_e) \\ &= G_s(X_0 + G_f F_e - X_e) \end{aligned} \tag{3.37}$$

The desired impedance is given by

$$X_e - X_0 = Z_d^{-1} F_e = G_d F_e \tag{3.38}$$

where Z_d is the desired (target) impedance characteristic. Here G_f must be designed to ensure the characteristics described by eq. 3.38. From the block diagram

$$X = G_m G_s(X_r - X_e) + G_m F_e$$

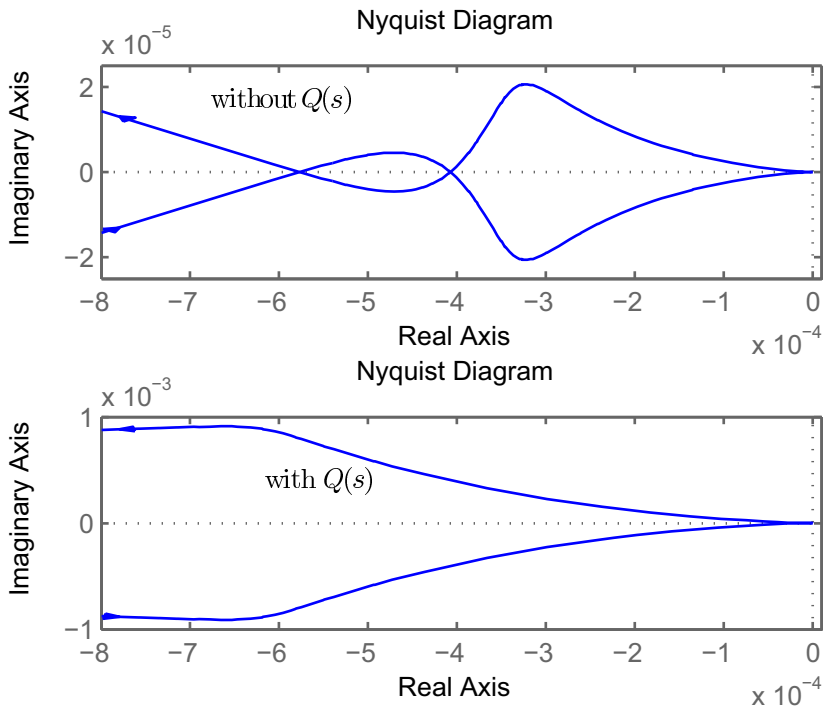

Figure 3.8: Nyquist plot of $T_{fb}(s)$: top–without $Q(s)$; bottom–with $Q(s)$ (for $m = 10, m_d = 1, b_d = 1.4, k_d = 1, Q = (0.01s + 1)/(0.1s + 1), G_b = 1/(15s^2 + 150s + 37500)$)

or

$$X_r = (G_m^{-1}G_s^{-1} + 1)X_e - G_s^{-1}F_e \tag{3.39}$$

Substitute eq. 3.39 into

$$\Delta X_0 = X_r - X_e$$

to obtain

$$\begin{aligned} \Delta X_0 &= (G_m^{-1}G_s^{-1} + 1)X_e - G_s^{-1}F_e - X_0 \\ &= (G_m^{-1}G_s^{-1} + 1)(G_dF_e + X_0) - G_s^{-1}F_e - X_0 \end{aligned}$$

Rearranging the above equation yields

$$\begin{aligned} \Delta X_0 &= G_m^{-1}G_s^{-1}X_0 + \left(\left(G_m^{-1}G_s^{-1} + 1\right)G_d - G_s^{-1}\right)F_e \\ &= G_m^{-1}G_s^{-1}X_0 + \left(G_p^{-1}G_d - G_s^{-1}\right)F_e \end{aligned} \tag{3.40}$$

where

$$G_p = \frac{G_sG_m}{1 + G_sG_m} \tag{3.41}$$

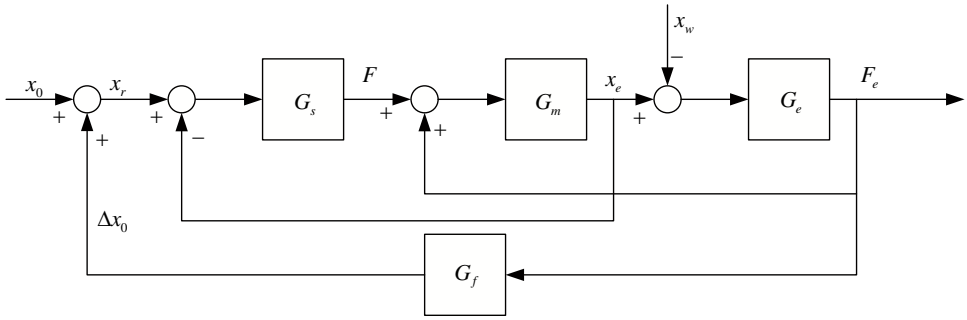

Figure 3.9: Block diagram of the position-based impedance control scheme

From eq. 3.40 to ensure the desired impedance characteristics

$$G_f = G_p^{-1} G_d - G_s^{-1} \tag{3.42}$$

For contact problem, without loss of generality, we may set the desired and static environment nominal positions to zero., i.e., $x_0 = 0, x_e = 0$. With these nominal values,

$$F = G_s(G_f F_e - X_e) \tag{3.43}$$

Effect of Base Motion

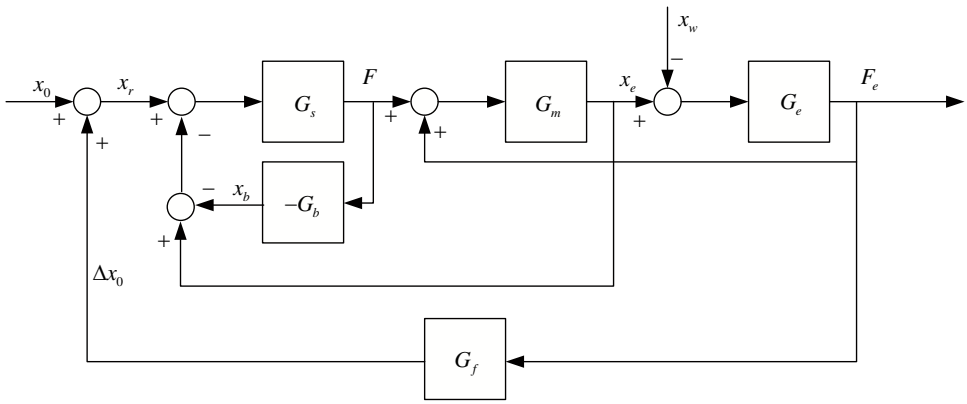

Figure 3.10: Block diagram of the position-based impedance control scheme in the FSMM

With the base motion, the measurement of the manipulator end-effector by on-board sensors is not X_e but instead $X_e - X_b$. The block diagram of the position-

based impedance control in the FSMM is shown in fig. 3.10. Here,

$$\begin{aligned} F &= G_s(G_f F_e - X_e + X_b) \qquad (3.44)\\ &= G_s(G_f F_e - X_e - G_b F) \\ F &= (1 + G_s G_b)^{-1} G_s G_f F_e - (1 + G_s G_b)^{-1} G_s X_e \qquad (3.45) \end{aligned}$$

Substituting into the equation of motion

$$\begin{aligned} F + F_e &= G_m^{-1} X_e \\ (1 + G_s G_b)^{-1} G_s G_f F_e - (1 + G_s G_b)^{-1} G_s X_e + F_e &= G_m^{-1} X_e \\ G_s G_f F_e + (1 + G_s G_b) F_e &= G_s X + (1 + G_s G_b) G_m^{-1} X_e \end{aligned}$$

or

$$\begin{aligned} T_{pb} = \frac{X_e}{F_e} &= \frac{1 + G_s G_b + G_s G_f}{(1 + G_s G_b) G_m^{-1} + G_s} \\ &= G_m \frac{1 + G_s G_b + G_s G_f}{1 + G_s G_b + G_s G_m} \qquad (3.46) \end{aligned}$$

Substituting eq. 3.42 into equation above and rearranging yields

$$T_{pb} = G_m \frac{G_s G_b + G_s G_d + G_d G_m^{-1}}{1 + G_s G_b + G_s G_m} \qquad (3.47)$$

In the case where the transfer function between the force and end-effector displacement is modeled as a simple mass, i.e.,

$$G_m = \frac{1}{ms^2}$$

the transfer function in eq. 3.47 is given by

$$\begin{aligned} T_{pb} &= \frac{1}{ms^2} \frac{G_s G_b + G_s G_d + ms^2 G_d}{1 + G_s G_b + \frac{G_s}{ms^2}} \\ &= \frac{1}{ms^2} \frac{G_b + G_d + ms^2 G_s^{-1} G_d}{G_b + G_s^{-1} + \frac{1}{ms^2}} \\ &= \frac{1}{ms^2} \frac{G_b + \left(G_s^{-1} + \frac{1}{ms^2}\right) ms^2 G_d}{G_b + \left(G_s^{-1} + \frac{1}{ms^2}\right)} \qquad (3.48) \end{aligned}$$

Let

$$A = \frac{1}{ms^2 G_d} \qquad (3.49)$$

and

$$B = \left(G_s^{-1} + \frac{1}{ms^2}\right)^{-1} \qquad (3.50)$$

Then,

$$\begin{aligned} T_{pb} &= \frac{X_e}{F_e} = \frac{1}{ms^2}\frac{G_b + B^{-1}A^{-1}}{G_b + B^{-1}} \\ &= \frac{1}{ms^2}\frac{1 + BAG_b}{A + BAG_b} \end{aligned} \tag{3.51}$$

This equation is in a similar form to eq. 3.27 in the force-based control. Actually, for

$$G_d = Z_d^{-1} = \frac{1}{m_d s^2 + K}$$

eq. 3.49 becomes

$$A = \frac{m_d s^2 + K}{ms^2} = \frac{m_d}{m} + \frac{K}{ms^2}$$

which is the same as eq. 3.28. Thus,

$$\begin{aligned} BA &= \left(G_s^{-1} + \frac{1}{ms^2}\right)^{-1}\left(\frac{m_d}{m} + \frac{K}{ms^2}\right) \\ &= \frac{\frac{m_d}{m} + \frac{K}{ms^2}}{\frac{1}{G_s} + \frac{1}{ms^2}} \\ &= \frac{ms^2 G_s}{ms^2 + G_s}\frac{m_d s^2 + K}{ms^2} \\ &= \frac{G_s\left(m_d s^2 + K\right)}{ms^2 + G_s} \end{aligned} \tag{3.52}$$

In terms of K

$$BA = K\left(\frac{\frac{m_d}{mK} + \frac{1}{ms^2}}{\frac{1}{G_s} + \frac{1}{ms^2}}\right)$$

Therefore, if G_s is selected such that

$$G_s = \frac{m}{m_d}K \tag{3.53}$$

then $BA \to K$. **In this case, the position-based impedance controller is equivalent to the force-based impedance controller**.

Similar to the force-based case, contact stability requires that

$$\angle\left(A(j\omega) + B(j\omega)A(i\omega)G_b(j\omega)\right) \neq \angle\left(1 + B(j\omega)A(i\omega)G_b(j\omega)\right), \quad \forall\omega > 0 \tag{3.54}$$

or similar to ineq. 3.31

$$\angle\left(A(j\omega) + e^{j\phi}g(\omega)\right) \neq \left(1 + e^{j\phi}g(\omega)\right), \quad \forall\omega > 0, \phi \tag{3.55}$$

for

$$|B(j\omega)A(j\omega)G_b(j\omega)| < g(\omega) \tag{3.56}$$

The uncertainty bound in this case is different from the one in the force-base case (in ineq. 3.30):

$$\begin{aligned} &\text{force-based:} && |K(j\omega)G_b(j\omega)| = |K(j\omega)|\,|G_b(j\omega)| \\ &\text{position-based:} && |B(j\omega)A(j\omega)G_b(j\omega)| = |B(j\omega)A(j\omega)|\,|G_b(j\omega)| \end{aligned}$$

Designing G_s

With high gain servo controller the uncertainty term $|B(j\omega)A(j\omega)G_b(j\omega)|$ can be much larger than $|K(j\omega)G_b(j\omega)|$ and will affect stability of the system. Consider a servo controller of the form

$$G_s = \alpha \frac{m}{m_d} K \tag{3.57}$$

where α is a scalar factor. For a passive function

$$K = b_d s + k_d$$

the servo controller is actually a PD controller. The form of $G(s)$ in eq. 3.57 deems appropriate as normally $K(s)$ would be designed to have good impedance behavior as would also be required for the servo controller. With this controller,

$$\begin{aligned} BA &= \frac{G_s\left(m_d s^2 + K\right)}{m s^2 + G_s} \\ &= \frac{\alpha \frac{m}{m_d} K\left(m_d s^2 + K\right)}{m s^2 + \alpha \frac{m}{m_d} K} \\ &= K \frac{\alpha\left(m_d s^2 + K\right)}{m_d s^2 + \alpha K} \end{aligned}$$

Then with $K(s) = b_d s + k_d$,

$$\begin{aligned} BA(j\omega) &= K(j\omega) \frac{(-\alpha m_d \omega^2 + \alpha k_d) + j\alpha b_d \omega}{(-m_d \omega^2 + \alpha k_d) + j\alpha b_d \omega} \\ |BA(j\omega)| &= |K(j\omega)| \left| \frac{(-\alpha m_d \omega^2 + \alpha k_d) + j\alpha b_d \omega}{(-m_d \omega^2 + \alpha k_d) + j\alpha b_d \omega} \right| \end{aligned}$$

The uncertainty bound of the position-based impedance controller will be greater than the uncertainty bound of the force-based impedance controller when

$$\begin{aligned} \left(-\alpha m_d \omega^2 + \alpha k_d\right)^2 &> \left(-m_d \omega^2 + \alpha k_d\right)^2 \\ \alpha^2 m_d^2 \omega^4 - 2\alpha^2 k_d m_d \omega^2 &> m_d^2 \omega^4 - 2\alpha m_d k_d \omega^2 \\ m_d \omega^2 \left(1 - \alpha^2\right) - 2\alpha k_d \left(1 - \alpha\right) &< 0 \\ m_d \omega^2 \left(1 + \alpha\right)\left(1 - \alpha\right) - 2\alpha k_d \left(1 - \alpha\right) &< 0 \end{aligned}$$

which can be divided into two cases according to the value of α:

- $\alpha < 1 \Rightarrow \omega < \sqrt{2\frac{k_d}{m_d}\frac{\alpha}{\alpha+1}}$
- $\alpha > 1 \Rightarrow \omega > \sqrt{2\frac{k_d}{m_d}\frac{\alpha}{\alpha+1}}$

Figure 3.11 shows plots comparing the magnitudes $|K(j\omega)|$ and $|B(j\omega)A(j\omega)|$ for several values of α. In general, for the servo controller we would expect to have α larger than 1. Therefore, in high frequency range the uncertainty bound of the position-based controller is expected to be larger than the uncertainty bound of the force-based controller. This will be critical if $|B(j\omega)A(j\omega)|$ is large in the frequency range close to natural frequencies of G_b.

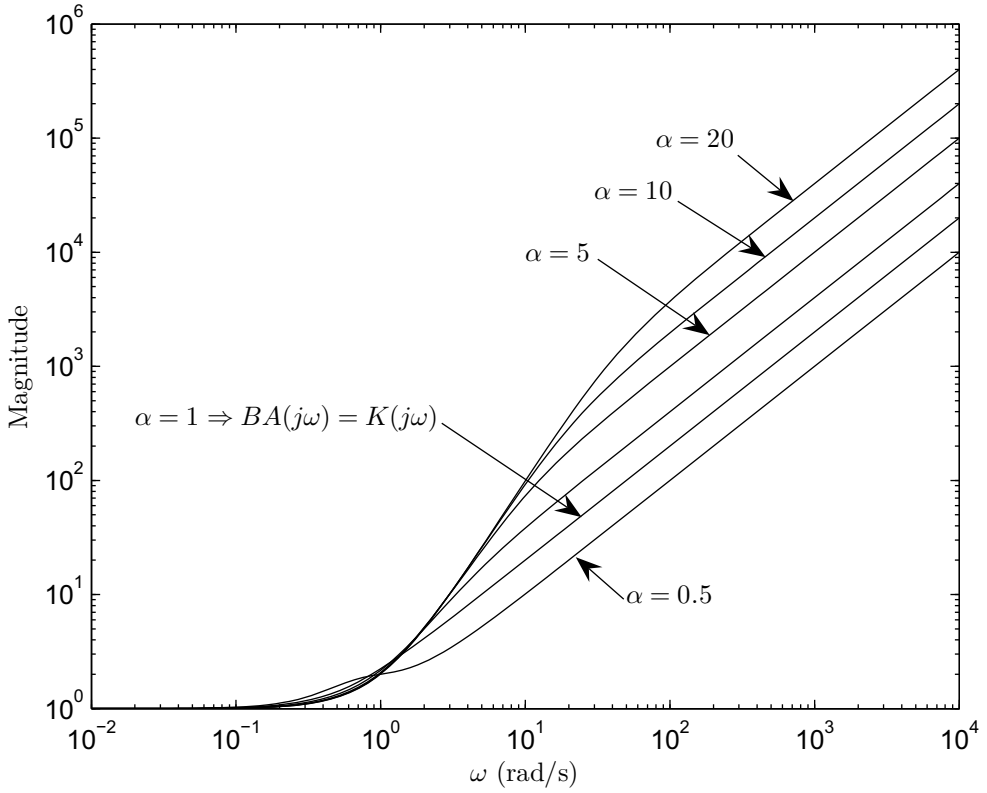

Figure 3.11: Plots of $|B(j\omega)A(j\omega)|$ (for $K(s) = 1.4s + 1, m_d = 1, m = 10, G_s = \alpha\frac{m}{m_d}K$)

Figure 3.11 shows plots of $|B(j\omega)A(j\omega)G_b(j\omega)|$ for several values of α . The base is assumed to be a simple spring-mass-damper system with $m_b = 15$ kg, $b_b =$

300 N.s/m, k_b = 37500 N/m which corresponds to a second order system with natural frequency 50 rad/s and damping ratio 0.2. The plot shows the magnitude of the bounds in which the greatest bound is at the natural frequency of the base. It is clearly seen that the larger the value of α the greater the uncertainty bound.

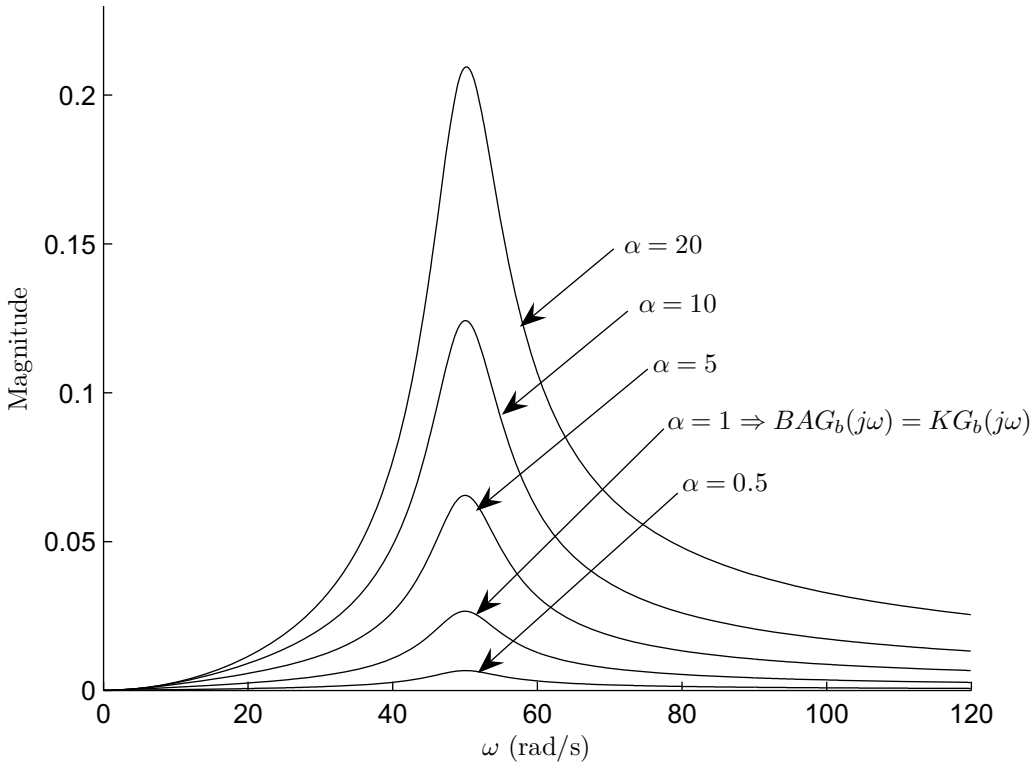

Figure 3.12: plots of $|B(j\omega)A(j\omega)G_b(j\omega)|$ (for $K(s) = 1.4s + 1, m_d = 1, m = 10, G_s = \alpha\frac{m}{m_d}K, G_b = \frac{1}{15s^2+300s+37500}$)

Robust controller design

Consider the control law

$$F = G_s(G_f F_e - X + X_b)$$

with

$$G_f = G_p^{-1}G_d Q^{-1} - G_s^{-1} = \frac{1 + G_s G_m}{G_s G_m}G_d Q^{-1} - \frac{1}{G_s} \tag{3.58}$$

where Q is an additional filter to be designed. With this control law, eq. 3.46 yields

$$\begin{aligned}
T_{pb} &= G_m \frac{1 + G_s G_b + G_s G_f}{1 + G_s G_b + G_s G_m} \\
&= G_m \frac{G_s G_b + \frac{G_d}{G_m} Q^{-1} + G_s G_d Q^{-1}}{1 + G_s G_b + G_s G_m} \\
&= \frac{1}{ms^2} \frac{G_s G_b + ms^2 G_d Q^{-1} + G_s G_d Q^{-1}}{1 + G_s G_b + \frac{G_s}{ms^2}} \\
&= \frac{1}{ms^2} \frac{G_b + G_d Q^{-1} + ms^2 G_s^{-1} G_d Q^{-1}}{G_b + G_s^{-1} + \frac{1}{ms^2}} \\
&= \frac{1}{ms^2} \frac{G_b + \left(G_s^{-1} + \frac{1}{ms^2}\right) ms^2 G_d Q^{-1}}{G_b + \left(G_s^{-1} + \frac{1}{ms^2}\right)} \\
&= \frac{1}{ms^2} \frac{G_b + B^{-1} A^{-1} Q^{-1}}{G_b + B^{-1}} \\
T_{pb} &= \frac{1}{ms^2} \frac{1 + BAQG_b}{AQ + BAQG_b}
\end{aligned} \tag{3.59}$$

The filter Q can be designed such that the magnitude of its frequency response function is small in the range where BAG_b is expected to be large, i.e. at the natural frequencies of G_b and also to keep the angle $\theta = \angle(1 - A(j\omega)Q(j\omega))$ as close to 90° as possible of for wide range of ω. Consider Q in the form of a lag-compensator

$$Q(s) = \frac{\tau_1 s + 1}{\tau_2 s + 1}$$

with $\tau_1 < \tau_2$. Here, $|Q(j\omega)|$ will drops below 1 after the corner frequency $\omega_a = 1/\tau_2$ with the rate of -20 dB/decade and will remain constant after $\omega_b = 1/\tau_1$. We can select τ_2 such that ω_a is less than the first natural frequency of the base. The lag compensator Q will also help to keep the angle θ larger when ω increases, thus providing robustness. Figure 3.13 shows the comparison of the uncertainty bound with and without the filter at $\alpha = 20$. As seen in the figure, the uncertainty bound can be reduced substantially with Q.

Figure 3.14 shows the plots of $AQ(j\omega)$ compared to $A(j\omega)$ for $\omega = [1, 120]$ rad/s. Here the magnitude and phase of $A(j\omega)$ is reduced by the effect of the filter Q. The phase of $AQ(j\omega)$ approaches 0° less quickly as ω increases and therefore the system is more robust. Figure 3.15 shows the Nyquist plots of T_{pb} with and without the filter Q. Note that the plot shown in the figure is an expanded

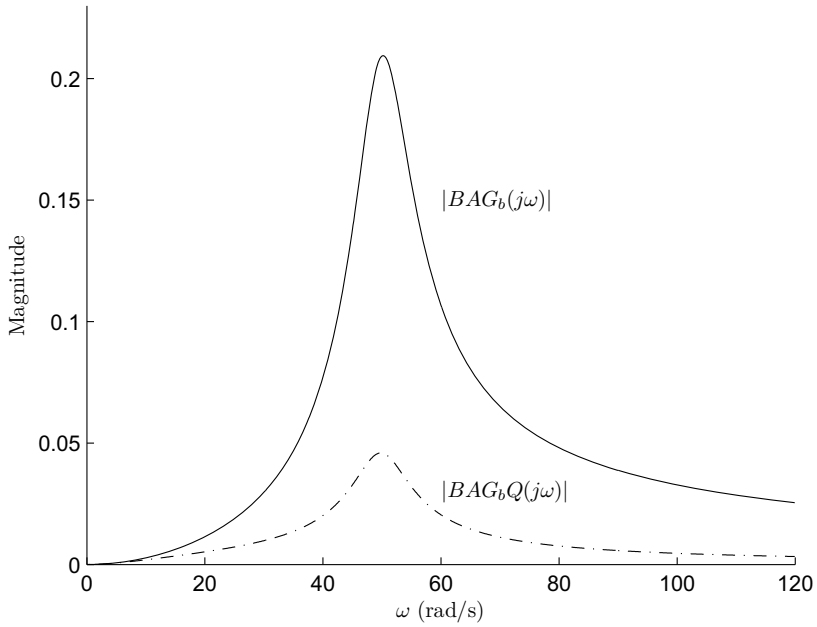

Figure 3.13: Comparison between the uncertainty bound with and without Q (for $K(s) = 1.4s + 1, m_d = 1, m = 10, G_s = 20\frac{m}{m_d}K, G_b = \frac{1}{15s^2+300s+37500}, \tau_1 = 0.01, \tau_2 = 0.1$)

view only in high frequency range. Without the filter Q, the Nyquist plot crosses the negative real axis and therefore in contact with wall, the system can become unstable. With the filter Q, the Nyquist plot does not cross the negative real axis for the entire frequency range and therefore, provided that T_{pb} is stable, the system is always stable in contact.

Although the filter Q can be used to increase the robustness, it can effect the performance of the system. Therefore it should be designed taking in mind this aspect as well. As in the example above, the design of such Q also gives good performance as shown fig. 3.16.

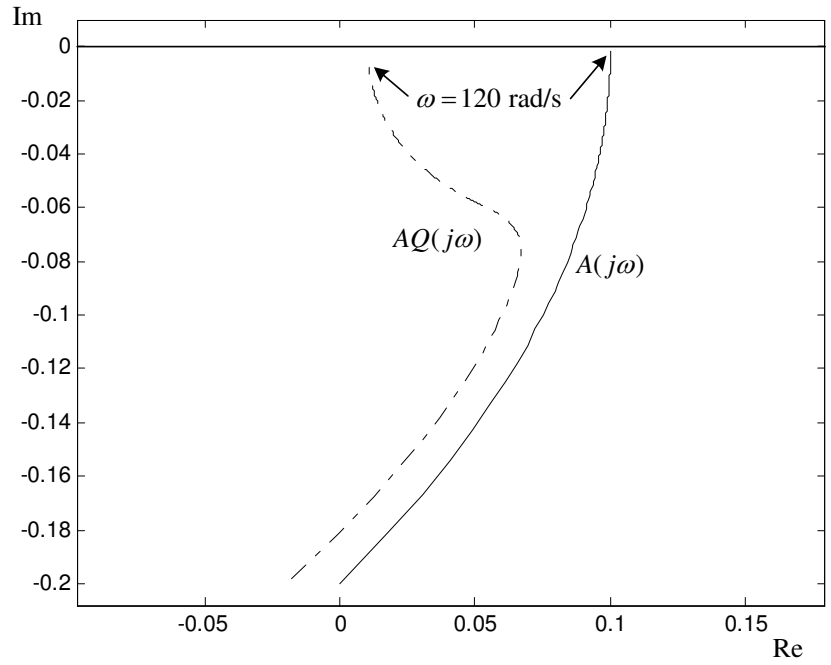

Figure 3.14: Plots of $A(j\omega)$ and $AQ(j\omega)$ (for $K(s) = 1.4s + 1, m_d = 1, m = 10, \tau_1 = 0.01, \tau_2 = 0.1$)

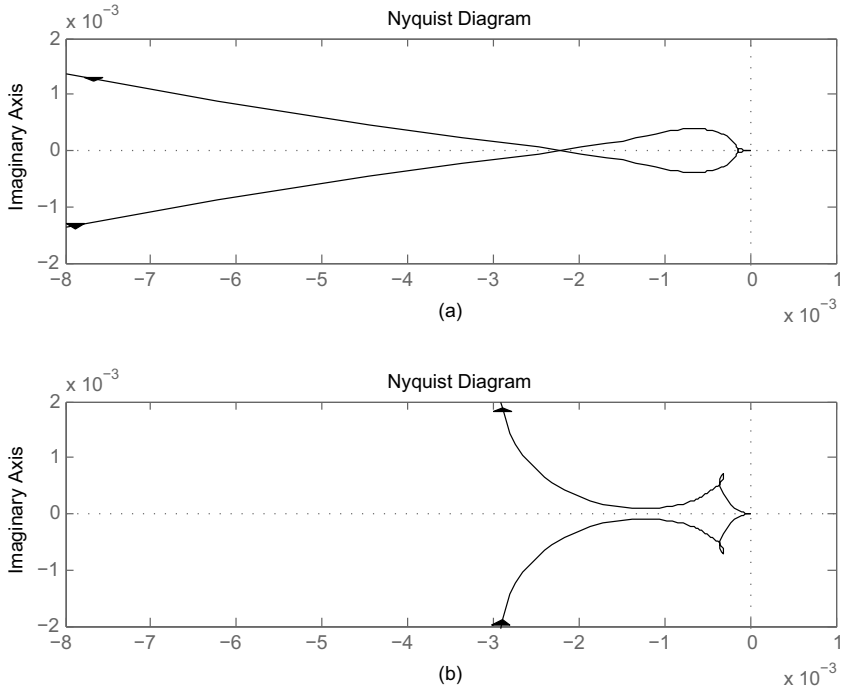

Figure 3.15: Nyquist plots of T_{pb} – in high frequency range (a) without filter Q (b) with filter Q (for $K(s) = 1.4s + 1, m_d = 1, m = 10, G_s = 20\frac{m}{m_d}K, G_b = \frac{1}{15s^2+300s+37500}, \tau_1 = 0.01, \tau_2 = 0.1$)

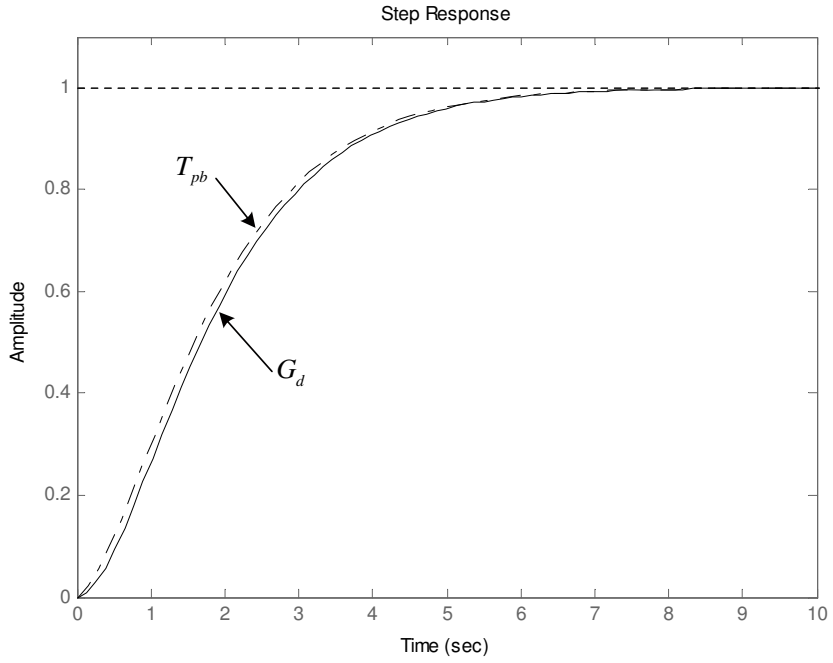

Figure 3.16: Step responses of: (solid) desired admittance G_d, (dash-dot) T_{pb} with Q (for $K(s) = 1.4s + 1, m_d = 1, m = 10, G_s = 20\frac{m}{m_d}K, G_b = \frac{1}{15s^2+300s+37500}, \tau_1 = 0.01, \tau_2 = 0.1$)

Chapter 4

Experimental Setup and Results

4.1 Experimental setup

4.1.1 A 2-DOF FSMM Test Rig

Figure 4.1 shows the drawing of a 2-DOF FSMM used for testing the control scheme. It composes of a rigid manipulator with two arms sitting on a platform which is made of a steel rectangular plate mounted, at its corners, to four long stainless poles. The first natural mode of vibration of the flexible structure is around 7 Hz. The arms of the manipulator travel on the horizontal plane and so is the vibration of the base. The manipulator arms are driven by d.c. motors through harmonic gear units. The angles of arm movement are measured by incremental encoders. Arm 1 has a counter mass attached to the opposite end to bring the center of mass closer to the arm joint. At the tip of arm 2, a six-axis force/torque sensor is installed to measure the force exerted by the wall during contact. Under the base, a two axis-accelerometer is installed to measure the base acceleration. The manipulator is installed near the wall so that the contact test can be performed. Figure 4.2 shows the picture of the 2-DOF FSMM that has been constructed and Table 4.1 lists the parameters of the system. The details and specifications of the sensors and motors are given in Appendix.

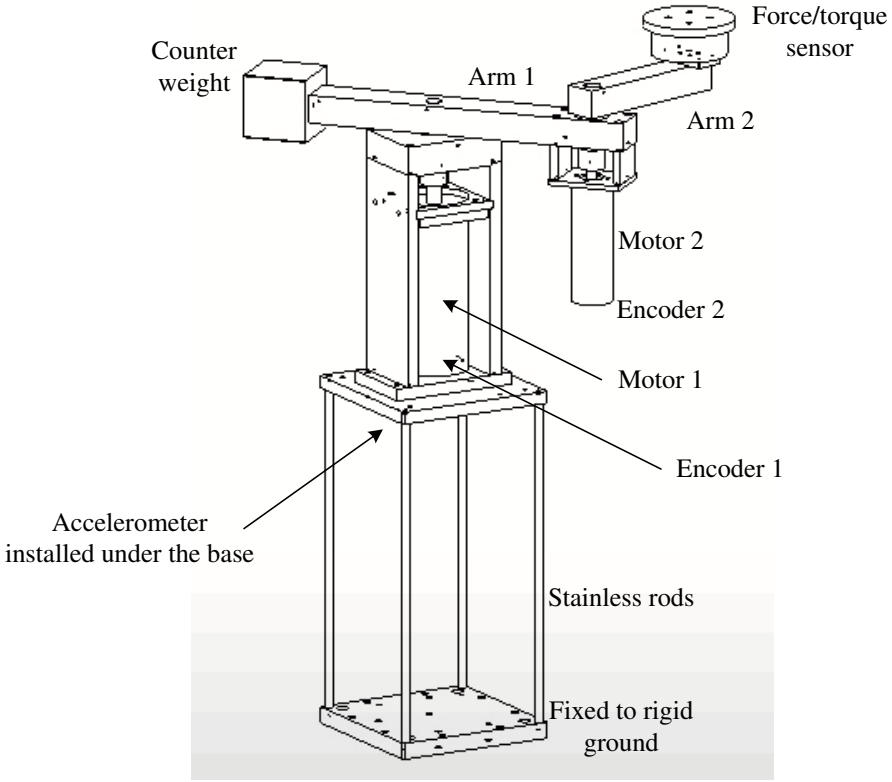

Figure 4.1: Drawing of a 2-DOF lab-scale FSMM

Figure 4.2: The 2-DOF lab-scale FSMM

Table 4.1: Parameters of the lab-scale FSMM

Item	Parameter
mass of arm 1	6.97 kg
mass of arm 2	2.76 kg
moment of inertia of arm 1 (reference to c.m.)	0.2262 kg.m^2
moment of inertia of arm 2 (reference to c.m.)	0.0098 kg.m^2
mass of the base	11.97 kg
length of arm 1	0.202 m
length of arm 2	0.1625 m
center of mass of arm 1 (measured from arm joint)	0.0524 m
center of mass of arm 2 (measured from arm joint)	0.1288 m

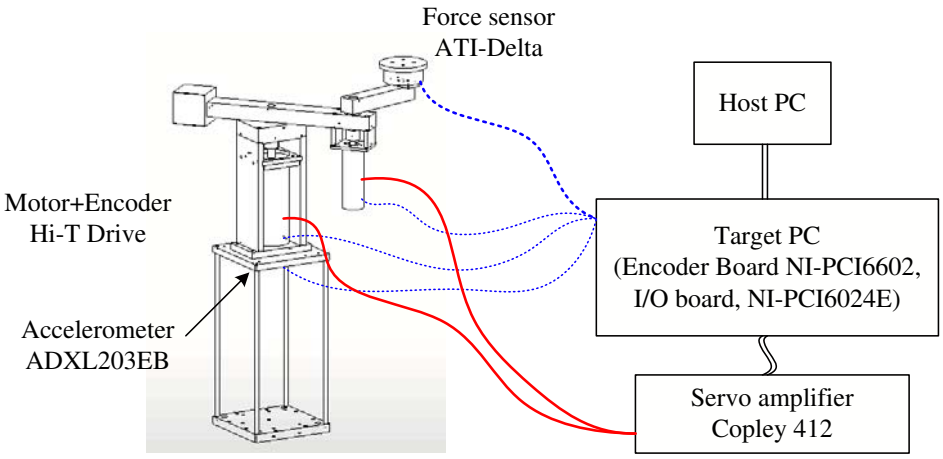

Figure 4.3: Experimental setup

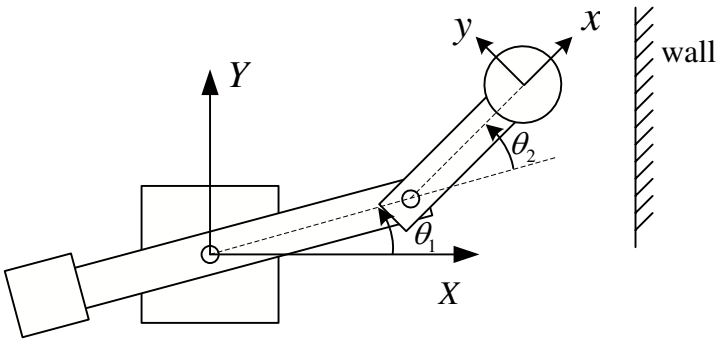

Figure 4.4: Coordinates of the FSMM

4.1.2 Experimental Setup

of

Figure 4.3 shows the diagram of the experimental setup. The control signal voltages are sent to the amplifiers which then supply the current proportional to the control signal to the motors. The sensors installed are as follows: 1) the encoders measure the angles of of rotation of the arms and send the signal to the encoder board installed in the computer 2) the force sensor measures the force exerted on the end-effector and sends the force signal to the I/O board also installed in the computer 3) the accelerometer measures the acceleration of the manipulator base and sends acceleration signals to the I/O board. The real-time signal is generated by the xPc Target system with MATLAB, Simulink and Real-Time-Workshops. The coordinates of manipulator base and the end-effector are defined corresponding to the diagram in fig. 4.4. Note that the wall has the surface normal vector in the direction opposite to the positive X axis.

4.1.3 Test Procedure

In order to test the performance of the control system, contact tests were performed. In the test, the end-effector of the manipulator was set up to initially touch the wall by giving an end-point reference command slightly inside the wall. The contact force and acceleration signals in the X-direction were then observed.

4.2 Results

4.2.1 Force-based control

In this experiment, many tests were performed for various sets of desired impedance parameters. The aim was to look for the conditions where unstable contacts can be observed and see how the robust controller can improve the stability. In some cases, the impedance controller could provide stable contact without $Q(s)$. And in other cases, the system were unstable. An example of the case where unstable contact occurs is when the desired impedance is set to $m_d = 50, b_d = 439.8, k_d = 1974.0$. Figure 4.5 shows the acceleration and contact force signals when the end-effector made contact with the wall. Here, mild vibrations in the system could be visually observed but the end-effector was still in contact with the wall. These vibrations can also be observed from the contact force signal with the amplitude fluctuating around $\pm$2.5N. In this case the system is unstable. Figure 4.6 shows the acceleration and contact force signals of another set up where the system was initially unstable as can be seen from fluctuation in the contact force signal. At time $t = 1$ second, $Q(s) = \frac{0.1s+1}{0.01s+1}$ was added to the controller. With $Q(s)$, the vibration in the system died out quickly and after a few second, the system settled down. Figure 4.7 shows the step responses of the system with impedance controller with $Q(s)$. The end-effector was initially set to contact the wall and had stable contact. At time $t = 1$ second, a step command was given so that the end-effector moved further into the wall. After the step command, the end-effector firstly reacted as if it would move out of the wall, but quickly it moved back into the wall and settled down with no vibration. From these plots, it is clear that $Q(s)$ improves stability of the system.

4.2.2 Position-based control

In this experiment, many tests were performed for various sets of desired impedance parameters and servo control parameters. In some cases, the impedance controller could provide stable contact without $Q(s)$. And in other cases, the system were unstable. An example of the case where unstable contact occurred is shown be-

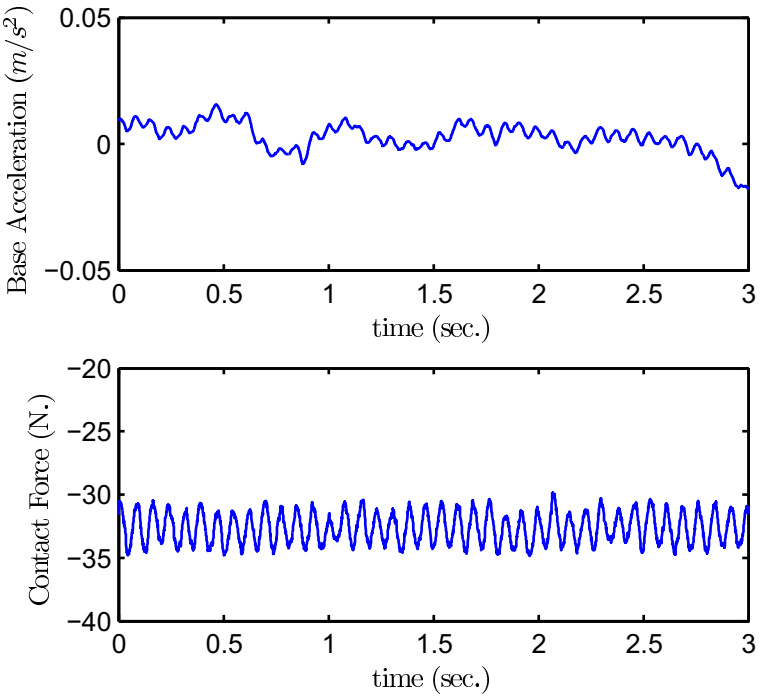

Figure 4.5: The plots of acceleration and contact force for the system with force-based impedance control shows unstable contact (no $Q(s)$ applied): $m_d = 50, b_d = 439.8, k_d = 1974.0$

low. Here, the desired impedance parameters were set to $m_d = 20, b_d =, k_d = 439.82, k_d = 3947.8$ which correspond to the spring-mass-damper system with natural frequency 2 Hz and damping ratio 0.7. The servo controller is a PD controller with $b_s = 560.3, k_s = 25148$ which correspond to α in eq. 3.57 being about 25. In the test, the manipulator's end-effector was set to initially touch the wall with some contact force. Then, at time $t = 1$ second the manipulator was given a step command on the end-effector position. The end-effector new set-point position was further inside the wall to create more contact force. Figure 4.8 shows the plots of the base acceleration and contact force signals. Initially, the contact force acting on the end-effector is about 17 N. After the step command, large vibration (visibly observable) occurred in the system as can be observed in the base acceleration and the contact force signals. At time $t = 6.2$ second, the filter $Q(s) = \frac{0.1s+1}{0.01s+1}$ was added to the controller. With $Q(s)$, the vibration disappeared quickly.

Figure 4.9 shows the step response for the case where $Q(s)$ was included from

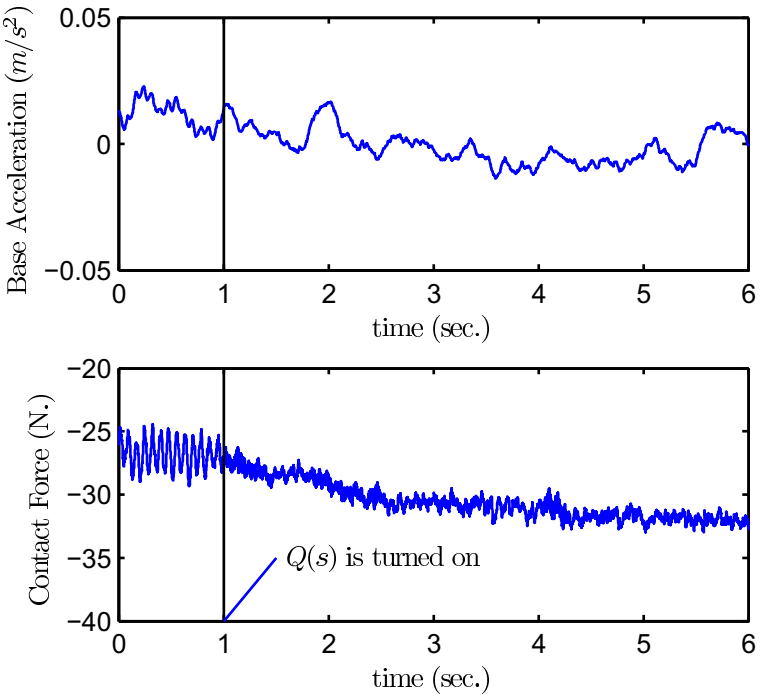

Figure 4.6: The plots of acceleration and contact force for the system with force-based impedance control shows stable contact after $Q(s)$ is applied : $m_d = 50, b_d = 439.8, k_d = 1974.0, Q = (0.01s + 1)/(0.1s + 1)$

the beginning. As can be observed, no vibration occurred in this case. Clearly, with $Q(s)$ the stability of the system is improved.

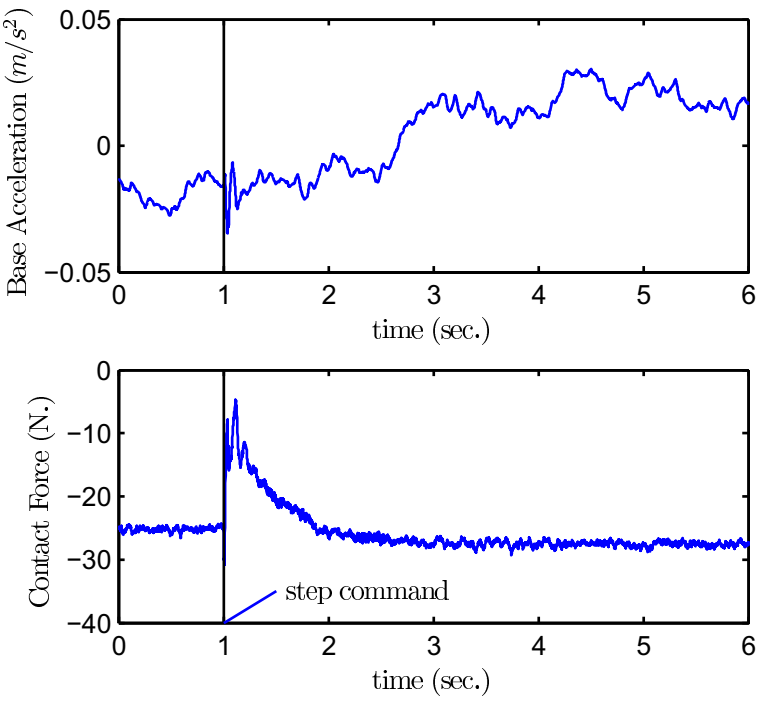

Figure 4.7: Step responses of the system with force-based impedance control with $Q(s)$: $m_d = 50, b_d = 439.8, k_d = 1974.0, Q = (0.01s + 1)/(0.1s + 1)$

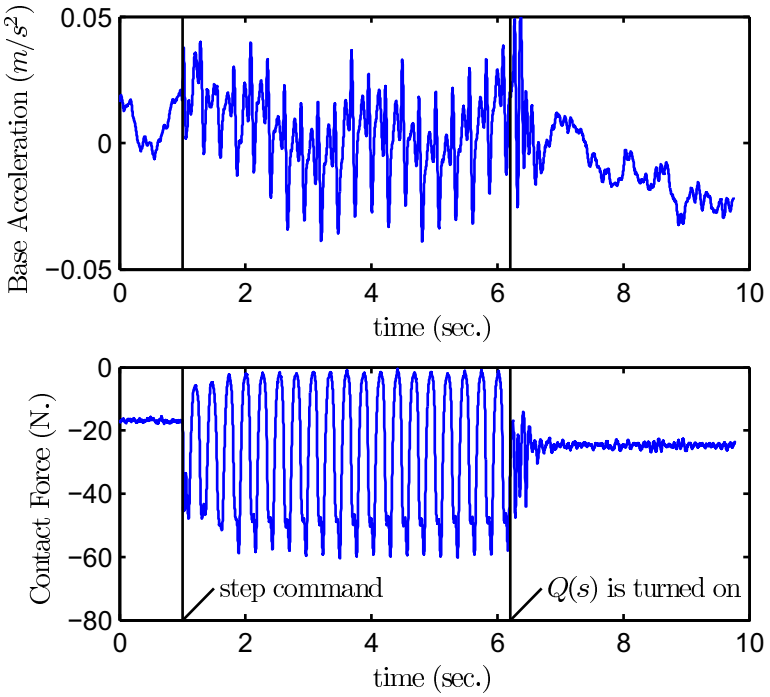

Figure 4.8: Step responses of the system with position-based impedance controller: $m_d = 25, b_d = 439.82, k_d = 3947.8, G_s = 560.3s+25148, Q(s) = (0.01s+1)/(0.1s+1)$

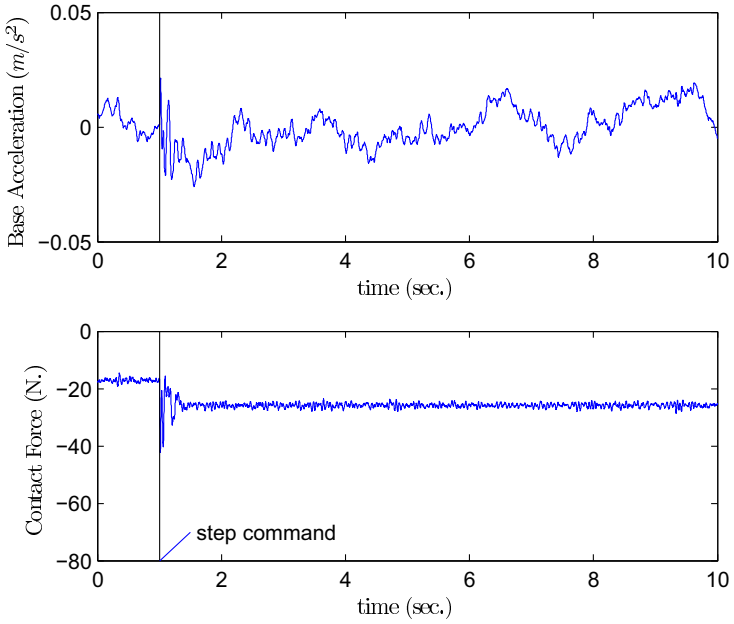

Figure 4.9: Step responses of the system with robust position-based impedance controller: $m_d = 25, b_d = 439.82, k_d = 3947.8, G_s = 560.3s + 25148, Q(s) = (0.01s + of1)/(0.1s + 1)$

Chapter 5

Conclusions

This research investigates force control techniques for flexible structure mounted manipulators performing contact tasks. Impedance control is the main subject of investigation. Two types of impedance control are studied: 1) force-based impedance control and 2) position-based impedance control. One-DOF contact model, along the surface normal direction, has been established. Based on the one-DOF model, the robust control schemes for both types of impedance control are derived. The goal is for the system to perform according to the desired impedance while remain stable when in contact with static environment such as wall. Based on the Nyquist stability criteria, the controllers are derived by ensuring that the Nyquist plots of the admittance of the controlled system do not cross the negative real axis. In order to verify the control schemes, a 2-DOF lab-scale flexible structure mounted manipulator has been constructed. Tests have been performed and the results show that the robust controllers can resolve the stability problems that occur under some conditions when non-robust controller are employed.

Although the controllers derived in this study can provide stable contact, the criteria employed are still conservative and therefore the contact performance may not be at its best. For further work, the robust performance during contact should be the main subject of study. Other issues such as joint flexibility, dynamic environment and friction should also be explored.

Bibliography

[1] D. S. Kwon, D. H. Hwang, S. M. Babcock and B. L. Burks, "Input shaping filter methods for the control of structurally flexible, long-reach manipulators," Proceedings of the 1994 IEEE International Conference on Robotics and Automation, San Diago, May 1993

[2] J. Y. Lew, "Contact control of flexible micro/macro manipulators," Proceedings of the 1997 IEEE International conference on robotics and automation, Albuquerque, New Mexico, April 1997

[3] J. Y. Lew and D.J. Trudnowski, "Vibration control of a micro/macro manipulator system," IEEE control system magazine, February 1996

[4] - D. P. Magee and W. J. Book, "Filtering schilling manipulator commands to prevent flexible structure vibration," Proceedings of the American Control Conference, Baltimore 1994

[5] - D. N. Nenchev, K. Yoshida and M. Uchiyama, "Reaction null-space based control of flexible structure mounted manipulator systems," Proceedings of the 35th Conference on Decision and Control, Kobe, Japan, Dec 1996

[6] - J. R. Sagli and O. Egeland, "Using momentum conservation to control linematically redundant manipulators," Modeling, Identification and Control, Vol 12 n.1, 1991

[7] - M. A. Scott and M. G. Gilbert "Active vibration damping of the space shuttle remote manipulator system," Journal of Guidance, Control and Dynamics, Vol. 16 n. 2, 1993

[8] - I. Sharf, "Active damping of a large flexible manipulator with short-reach robot," Journal of Dynamic Systems, Measurement and Control, Vol. 118, Dec 1996

[9] - M. A. Torres and S. Dubowsky, "Path-planning for elastically constrained space manipulator systems," Proceedings of the 1993 IEEE International Conference on Robotics and Automation, Atlanta GA, May 1993

[10] - M. A. Torres, S. Dubowsky and A. C. Pisoni, "Path planning for elastically-mounted space manipulators: experiment evaluation," Proceedings of the 1994 IEEE Internal Conference on Robotic and Automation, San Diago, CA, May 1994

[11] - K. Yoshida, D.N. Nenchev, and M. Uchiyama, "Vibration suppression and zero reaction maneuvers of flexible space structure mounted manipulators," Smart Materials and Structures, Vol. 8, 1999

Outputs

The results of this research work help to understand the theory outlining the impedance control of a flexible structure mounted manipulator performing contact tasks. The author has been writing an article to submit to an academic journal. The title of the article will be "Robust impedance controls for flexible structure mounted manipulator performing contact tasks". The writing of the article should be finished within two months from the date posted in this report.

Appendix A

Specifications of Sensors and Actuators

Table A.1: Specifications of Force Sensors

Item	**Details**	
Made	ATI INDUSTRIAL AUTOMATION	
Model	Delta US-150-600	
Sensing ranges		
F_x, F_y (±N)	660	
F_z (±N)	1,980	
T_x, T_y (±N-m)	60	
T_z (±N-m)	60	
Resolution	Controller F/T System	16 bit DAQ F/T System
F_x, F_y (±N)	1/2	1/32
F_z (±N)	1	1/16
T_x, T_y (±N-m)	3/100	3/1,600
T_z (±N-m)	3/100	3/1,600
Single-axis overload		
F_x, F_y (±N)	3,400	
F_z (±N)	12,000	
T_x, T_y (±N-m)	220	
T_z (±N-m)	420	
Resonant frequency		
F_x, F_y, T_z	1,500 Hz	
F_z, T_x, T_y	1,700 Hz	
Physical specifications		
Weight	910 g	
Diameter	94.5 mm	
Height	33.3 mm	
Temperature Error (from 22°C)	Typical gain error	
±5°C	0.1%	
±15°C	0.5%	
±25°C	1%	
±50°C	5%	

Table A.2: Motor Specifications

Item	**Motor 1**	**Motor 2**
Made	Harmonic Drive	Harmonic Drive
	System Inc.	System Inc.
Model	RH-20-3004-OEM	RH-14GH11OEM
Rate output power (W)	90	20.3
Rate current (A)	3	1.8
Peak current (A)	15	5.4
Torque constant (Nm/A)	18.121	2.602
Moment of inertia (kg.m^2)	0.000026 (armature)	0.0021
Weight with encoder (kg)	3.02	0.78
Gear ratio	1/100	1/50
Encoder		
Resolution (ppr)	1,000	1,000
Output signal	A, A/, B, B/, Z, Z/	A, B, Z,
Power supply (VDC)	+5V TTL open collector	+5V TTL open collector
Max.output current (mA)	20	20
Max. signal freq. (kHz)	100	100

Table A.3: Specifications of accelerometer

Item	**Specification**
Made	Analog Devices
Model	ADXL203EB
No. of Axis	2
Range	±1.7g
Sensitivity	1000 mV/g
Sensitivity accuracy	±6
Output type	Analog
Bandwidth	2.5 kHz
Noise density	110
Supply current	0.7 mA
Supply voltage	3 to 6 VDC
Temp range	-40°C to 125°C
Package	E-8